Journal of Engineering for Gas Turbines and Power

Copy of e-mail Notification

Journal of Engineering for Gas Turbines and Power Published by ASME
Dear Author,
Congratulations on having your paper accepted for publication in the ASME Journal Program.
Your page proof is available in PDF format from the ASME Proof Download & Corrections site here:
http://115.111.50.156/jw/AuthorProofLogin.aspx?pwd=10debfc26a8b&CA=AS

Login: your e-mail address
Password: 10debfc26a8b

Please keep this email in case you need to refer back to it in the future.
You will need Adobe Acrobat Reader software to view the file. This is free software and a download link is provided when you log in to view your proofs.

Responsibility of detecting errors rests with the author. Please review the page proofs carefully and:
1. Answer any queries on the first page "Author Query Form"
2. Proofread any tables and equations carefully
3. Check to see that any special characters have translated correctly
4. Publication will not proceed until a response is received. If there are no corrections, a response is still required.

RETURNING CORRECTIONS:
Corrections must be returned using the ASME Proof Download & Corrections Submission Site (link above). You will be able to upload:
1. Annotated PDF
2. Text entry of corrections, with line numbers, in the text box provided
3. Additional files, if necessary.

SPECIAL NOTES:
Your Login and Password are valid for a limited time. Please reply within 48 hours.

Corrections not returned through the above website will be subject to publication delays. This e-proof is to be used only for the purpose of returning corrections to the publisher. If you have any questions, please contact: asme.cenveo@cenveo.com, and include your article no. (GTP-15-1438) in the subject line. This email should not be used to return corrections.

Approval of these proofs re-confirms the copyright agreement provision that all necessary rights from third parties for any copyrighted material (including without limitation any diagrams, photographs, figures or text) contained in the paper has been obtained in writing and that appropriate credit has been included.

Sincerely,
Mary O'Brien, Journal Production Manager

STATEMENT OF EDITORIAL POLICY AND PRACTICE

The Technical Committee on Publications and Communications (TCPC) of ASME aims to maintain a high degree of technical, literary, and typographical excellence in its publications. Primary consideration in conducting the publications is therefore given to the interests of the reader and to safeguarding the prestige of the Society.

To this end the TCPC confidently expects that sponsor groups will subject every paper recommended by them for publication to careful and critical review for the purpose of eliminating and correcting errors and suggesting ways in which the paper may be improved as to clarity and conciseness of expression, accuracy of statement, and omission of unnecessary and irrelevant material. The primary responsibility for the technical quality of the papers rests with the sponsor groups.

In approving a paper for publication, however, the TCPC reserves the right to submit it for further review to competent critics of its own choosing if it feels that this additional precaution is desirable. The TCPC also reserves the right to request revision or condensation of a paper by the author or by the staff for approval by the author. It reserves the right, and charges the editorial staff, to eliminate or modify statements in the paper that appear to be not in good taste and hence likely to offend readers (such as obvious advertising of commercial ventures and products, comments on the intentions, character, or acts of persons and organizations that may be construed as offensive or libelous), and to suggest to authors rephrasing of sentences where this will be in the interest of clarity. Such rephrasing is kept to a minimum.

Inasmuch as specific criteria for the judging of individual cases cannot, in the opinion of the TCPC, be set up in any but the most general rules, the TCPC relies upon the editorial staff to exercise its judgment in making changes in manuscripts, in rearranging and condensing papers, and in making suggestions to authors. The TCPC realizes that the opinions of author and editor may sometimes differ, and hence it is an invariable practice that no paper is published until it has been passed on by the author. For this purpose page proofs of the edited paper are sent to the author prior to publication in a journal. Changes in content and form made in the proofs by authors are followed by the editor except in cases in which the Society's standard spelling and abbreviation forms are affected.

If important differences of opinion arise between author and editor, the points at issue are discussed in correspondence or interview, and if a solution satisfactory to both author and editor is not reached, the matter is laid before the TCPC for adjustment.

Technical Committee on Publications and Communications (TCPC)
Reviewed: 05/2012

AUTHOR QUERY FORM

ASME SETTING THE STANDARD	**Journal: J. Eng. Gas Turbines Power** **Article Number: GTP-15-1438**	**Please provide your responses and any corrections by annotating this PDF and uploading it to ASME's eProof website as detailed in the Welcome email.**

Dear Author,

Below are the queries associated with your article; please answer all of these queries before sending the proof back to Cenveo. Production and publication of your paper will continue after you return corrections or respond that there are no additional corrections.

Location in article	Query / Remark: click on the Q link to navigate to the appropriate spot in the proof. There, insert your comments as a PDF annotation.
AQ1	Reminder – the ASME Copyright Agreement that was signed by all authors includes the following: "You have the right to enter into this Copyright Form and to make the assignment of rights to ASME. If the Paper contains excerpts from other copyrighted material (including without limitation any diagrams, photographs, figures or text), you have acquired in writing all necessary rights from third parties to include those materials in the Paper, and have provided appropriate credit for that third-party material in footnotes or in a bibliography." As required, ASME may contact the authors to obtain a copy of the written permission.
AQ2	Any content obtained from the web and included in the paper may require written permission and appropriate credit if it is copyrighted content. If copyright status cannot be determined, this content should not be included in the paper.
AQ3	As per the journal style three or fewer letters acronyms are not allowed in the title; therefore, we have replaced the acronym CFD with the spelled out definition.
AQ4	Please define CAD and RGB at first occurrence.
AQ5	Please reword text without color words as readers of print will only see black and white figures.
AQ6	Kindly specify which section "in the previous section" refers to here.
AQ7	Please specify which section or subsection "in the following section" refers to here.
AQ8	Refs. 26 and 27 was not cited in text. Please check its insertion here.
AQ9	Please specify which section or subsection "in the previous section" refers to here.
AQ10	Kindly provide DOI for Refs. 5, 6, 12, 24, 25.
AQ11	Kindly provide Issue for Refs. 8, 9, 19, 21.

Thank you for your assistance.

J_ID: GTP DOI: 10.1115/1.4031760 Date: 13-October-15 Stage: Page: 1 Total Pages: 10

PROOF COPY [GTP-15-1438]

AQ1
AQ2

A Shape Memory Alloy-Based Morphing Axial Fan Blade—Part II: Blade Shape and Computational Fluid Dynamics Analyses

Alessio Suman[1]
Fluid Machinery Research Group,
Engineering Department in Ferrara (ENDIF),
University of Ferrara,
Ferrara 44122, Italy

AQ3

Annalisa Fortini
Metallurgy Research Group,
Engineering Department in Ferrara (ENDIF),
University of Ferrara,
Ferrara 44122, Italy

Nicola Aldi
Fluid Machinery Research Group,
Engineering Department in Ferrara (ENDIF),
University of Ferrara,
Ferrara 44122, Italy

Mattia Merlin
Metallurgy Research Group,
Engineering Department in Ferrara (ENDIF),
University of Ferrara,
Ferrara 44122, Italy

Michele Pinelli
Fluid Machinery Research Group,
Engineering Department in Ferrara (ENDIF),
University of Ferrara,
Ferrara 44122, Italy

The ability of a morphing blade to change its geometry according to the different operating conditions represents a challenging approach for the optimization of turbomachinery performance. In this paper, experimental and computational fluid dynamics (CFD) numerical analyses on a morphing blade for a heavy-duty automotive cooling axial fan are proposed. Starting from the experimental results proposed in the first part of this work, a morphing blade, made of shape memory alloy (SMA) strips embedded in a polymeric structure, was thoroughly tested. In order to assess the ability of the strips to reach a progressive and smooth shape changing evolution, several experiments were performed in a purpose-built wind tunnel. The morphing blade changed its shape as the strips were thermally activated by means of air stream flow. The bending deformation evolution with the increasing number of thermal cycles was evaluated by digital image analysis techniques. After the analyses in the wind tunnel, CFD numerical simulations of a partially shrouded fan composed of five morphing blades were performed in order to highlight the evolution of the fan performance according to air temperature conditions. In particular, the capability of the blade activation was evaluated by the comparison between the fan performance with nonactivated blades and with activated blades. The results show a progressive stabilization of the shape memory behavior after the first cycle. The blade deformation led to a significant improvement in the fan performance at a constant rotational velocity. The CFD numerical simulation points out the differences in the overall performance and of three-dimensional fluid dynamic behavior of the fan. This innovative concept is aimed at realizing a sensorless smart fan control, permitting (i) an energy saving that leads to fuel saving in the automotive application fields and (ii) an increase in engine life, thanks to a strong relationship between the engine thermal request and the cooling fan performance. [DOI: 10.1115/1.4031760]

Introduction

More than half of the energy in vehicles is lost as heat to the different cooling systems (engine cooling system, air conditioning, frictional components cooling, etc.) and exhaust gas. Reducing the amount of energy lost in vehicle cooling systems enhances the efficiency of the vehicles as reported by Lin and Sunden [1]. A traditional cooling system is made up of (i) pump, (ii) thermostat valve, (iii) heat exchanger, and (iv) cooling fan.

The cooling system has to simultaneously balance engine thermal management, passenger thermal comfort, and cooling system parasitic losses over all vehicle operating conditions and climate control demands. For a given vehicle application (high and low velocity vehicle, truck and heavy-duty engine), the cooling system technologies evaluated for heater performance are selected with regard to the entire cooling system and thermal management objectives, such as [2]: (i) peak cooling system performance, (ii) fast engine warm-up, (iii) precise coolant temperature control, (iv) thermal comfort, (v) improved fuel economy, (vi) reduced thermal shocks, and finally, (vii) low cost. These objectives are met by robust and efficient design including an efficient controllable water pump and electric fan, a high-performance heat exchanger with low pressure drops (air and water side) and an electric flow control valve for precise temperature control during the transient engine load through different ambient temperatures.

In order to improve the engine thermal management, many different methods have been developed in recent years: electric heaters, electric water pumps, heat pumps, and fuel-fired coolant heaters. These systems vary in terms of performance, packaging considerations, reliability, costs, and auxiliary devices to support them.

In automotive applications, conventional cooling systems are generally not very accurate, not controllable and lead to considerable parasitic losses. In most cases, fans and water pumps have great difficulty in correctly monitoring and maintaining multiple operating temperature levels [3]. Cooling systems are designed to simply guarantee sufficient heat removal at maximum engine output conditions in the worst vehicle operating conditions (low vehicle velocity and high temperature ambient). Unfortunately, these operational conditions only represent approximately 5% of the conditions that the cooling system encounters during its operation [4]. In fact, the engine cooling system is significantly influenced by cooling air generated by (i) a ram effect resulting from the vehicle's motion and (ii) suction produced by fan operation [5]. The combined effect of these two factors is highly variable and their coupling with the cooling fan and pump presents a target which is difficult to reach.

The present work focuses on an innovative passive control system for the performance optimization of an automotive axial cooling fan. The fan is regulated by a sensorless control taking

[1]corresponding author.

Contributed by the Turbomachinery Committee of ASME for publication in the Journal of Engineering for Gas Turbines and Power. Manuscript received September 3, 2015; final manuscript received September 16, 2015; published online xx xx, xxxx. Editor: David Wisler.

ID: **asme3b2server** Time: 13:16 I Path: //chenas03/Cenpro/ApplicationFiles/Journals/ASME/GTP#/Vol00000/150219/Comp/APPFile/AS-GTP#150219

advantage of the SMA elements embedded in the polymeric blade structure.

Material selection and characterization, blade design, and preliminary activation tests are reported in the first part [6] which focused in particular on the description of the blade deformation and activation time.

This second part focuses on (i) the progressive stabilization of the shape memory behavior after the first cycle and (ii) the fluid dynamic phenomena induced by blade camber variation due to the SMA strips actuation. The fan performance variation, related to the blade modification is studied by using CFD numerical simulations. The numerical model takes into account the different blade shapes, thanks to an innovative instant three-dimensional blade shape detection provided during the activation tests of the blade. The coupling of different fan rotational velocities and different blade shapes is the basis for the multiple surface performance map reported in this second part.

Literature Survey

The thermal management of an engine is related to the efficient control of the thermal energy flows in accordance with the specific requirements and the prevailing operating conditions. Proper thermal management is reflected in a reduction of vehicle emissions and fuel consumption and in an improvement of the mechanical engine efficiency and life. As reported in Ref. [7], proper management of the cooling system can reduce (i) the warm-up time, (ii) the pollutant emissions, and (iii) the size of the cooling system compared to an increase of engine efficiency and operation life due to the correct control of postcooling (avoiding the heat soak).

In order to reach these advantages, two strategies can be adopted: (i) single component optimization (heat exchange, cooling fan, water pump, etc.) or (ii) entire system optimization (engine, cooling circuit, etc.).

In literature, a single component optimization is widespread [8]. The optimization can be developed through the use of the one-dimensional analytical model or it is possible to couple the one-dimensional model with CFD. For example, in Ref. [9] parametric studies on automotive heat exchangers are reported. Oliet et al. [9] studied the overall behavior of automobile heat exchangers working at a usual range of operating conditions. The results highlight the importance of the air inlet flow rate and of the temperature in the overall heat transfer coefficient. In this sense, the under-hood air flow management is one of the most important fields of research. In fact, the automotive development trend moves toward the increase in engine power and the decrease of under-hood space in favor of driver and passenger compartment space [10]. Besides, the under-air flow has a negative effect on the total drag. The cooling air drag can be as large as 8% of the total air resistance [10]. In support of this, the fan-to-radiator spacing and fan-to-engine spacing play a key role in the cooling circuit performance. The air flow at the front of the vehicle, passes through the grille, condenser, radiator, cooling fan, and other components, removing the rejected heat to the surrounding environment [5]. The cooling fan operates in a blockage condition due to the upstream radiator and downstream engine, and for these reasons, the axial fan works with a higher radial flow.

The space-optimization of the engine bay has to take into account two main aspects: the cooling system capability and the aerodynamic performance of the vehicle. Particular attention is given to off-design conditions, such as off-highway heavy-duty truck operation [11] and postcooling of the engine after high engine loads [12].

The air-side optimization of the cooling system is not the only strategy to meet the increasing demand of energy efficiency. The water side of the cooling system could also be subjected to optimization. In Ref. [13], a different control strategy of the water thermostat improves the engine efficiency during the transient operation (warm-up). The cooling system is also optimized considering many components at the same time. As reported in Ref. [7], active coolant control (by means of electronic water pump and valves) substantially contributed to a reduction of coolant warm-up time during the cold engine start as well as the emission and fuel consumption. The active control avoids the frequent changes in the coolant temperature that exist when the passive control system is used.

In this background, a cooling fan controlled by the SMA devices could be an innovative solution in order to exclude electric motor, sensor, cable connection, and all of the electronic devices in the vehicle structure. Furthermore, the SMA device driven by the air temperature matches with the new control strategy that refers to a coolant control strategy by using temperature instead of engine rotational velocity. The fan performance is related to the air flow temperature during the warm-up, standard operation, and after-load engine operating conditions. For these reasons, this new concept represents one of the most interesting challenges in automotive applications. Examples of adaptive structures regard the improvement of the global efficiency of aircraft wings [14], helicopter blades [15], and wind turbines [16]. However, no study addresses the use of SMA elements as actuators in fan blades. In this work, the authors have reported an extended analysis of the blade, realized as a functional structure with the embedded NiTi SMA strips, and its stabilization due to repeated thermal cycling. The blade shape analysis is provided by using (i) the digital image analysis technique and (ii) an innovative three-dimensional blade surface detection. After the blade shape analysis, numerical CFD simulations are conducted in order to establish the capability of the SMA activation to induce the variation of the fan performance. Different fan rotational velocities are investigated and the modulating capability of the SMA elements is also highlighted.

Experimental Apparatus

The experimental apparatus, named single blade test facility (SBTF), includes numerous temperature sensors, velocity sensors, and digital image devices, and allowed the characterization of the morphing blade.

Morphing Blade Structure. The structure was designed in order to be sufficiently compliant and flexible to support the large deflections induced by the strips and to allow the shape recovery, but also stiff enough to withstand aerodynamic loads. The chosen blade structure was a mixture of Nylon PA 6.6, glass fibers and elastomer. The embedded SMA strips had a nominal composition of $Ni_{50.2}Ti_{49.8}$, with a thickness equal to 1.5 mm and they were put in contact with the fluid flow by means of several slots. In Fig. 1, the blade sketch, with the essential region, is reported. The SMA characterization and the comparative results between the polymeric matrices are reported in the first part of this work [6].

Thermal Cycle. The SMA thermal activation was achieved by (i) a heating ramp and (ii) a cooling ramp, described as follows. Starting from room temperature the blade was firstly heated by a hot air stream flow, which caused the activation of the SMA strips and the blade deflection. The blade reached the maximum deflection as the fluid flow reached the maximum temperature. Subsequently, the blade was cooled to room temperature.

SBTF. As depicted in Fig. 1, the SBTF was composed of (i) a convergent device, (ii) a polyvinyl chloride (PVC) pipe, (iii) a flow straightener, (iv) a polymethyl methacrylate (PMMA) transparent measurements section, and (v) an exhaust pipe. The wind tunnel was driven by an axial fan with a nominal 1500 m^3/h flow rate that provided the air flow stream through a 22-kW electric heater. With the SBTF, it was possible to realize a highly reproducible timewise thermal gradient, which can reach values of up to about 12 °C/min in heating mode and up to about 6 °C/min in cooling mode. These temperature gradients are consistent with the

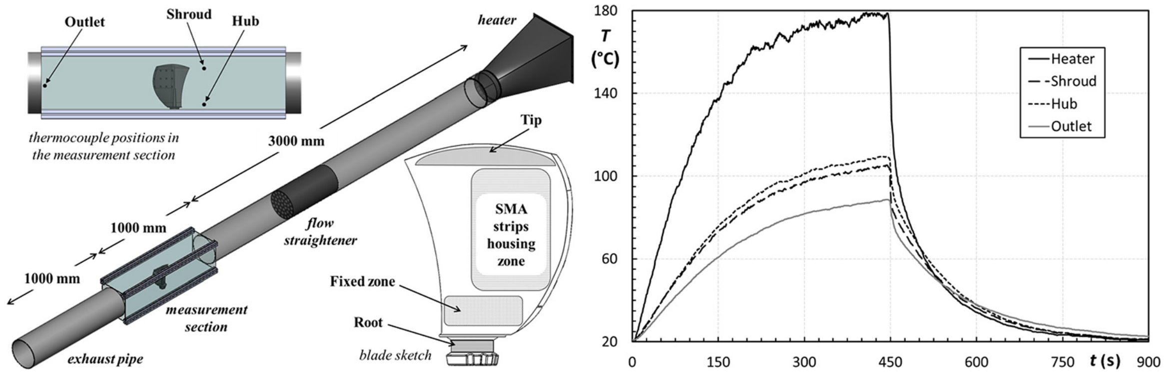

Fig. 1 SBTF functional scheme and its thermal performance

operating conditions of the fan when used in normal duty. More details can be found in the previous paper [6].

In order to evaluate the thermofluid dynamic conditions, a hot wire anemometer, a pitot static tube, and several calibrated thermocouples were installed in the SBTF. In particular, the thermocouples for the control of the air flow were placed in correspondence to the heater, in the vicinity of the blade (at the shroud and hub positions), and at the outlet section as can be seen in Fig. 1. Temperature and velocities were constantly monitored during the activation test. Several welded tip thermocouples type K were also placed on the blade surface and on the SMA strips to acquire the temperature evolution.

Figure 1 shows the experimental temperature evolution as a function of time in correspondence to the sections illustrated in the sketch. Thanks to the transparency of the measurements section, the evolution of the blade shape was continuously evaluated by means of digital image analysis techniques. Three digital cameras were aligned in correspondence to the blade tip, suction side, and pressure side, respectively. In addition, the three-dimensional blade shape was acquired during the tests by using the Microsoft Kinect sensor. The temperature acquisition was synchronized with the video acquisition (1024×768) pixels and the three-dimensional blade surface acquisition in order to control the overall change in blade shape related to the temperature trend.

Blade Shape Scan. In addition to digital images and video analyses, the three-dimensional blade shape was detected by the Microsoft Kinect sensor. This is a motion sensing camera, released as a peripheral device for the Xbox360 console and Windows, which is capable of providing streaming noncontact depth information and color information at a resolution of (640×480) pixels with a rate of 30 frames per second. The Kinect contains (i) an RGB sensor imaging made up of double camera arrangement; (ii) an infrared (IR) emitter and an IR depth sensor; and (iii) a three-axis accelerometer to control its orientation. Since traditional 3D motion capture systems are generally complex and very expensive, the Kinect-based 3D surface imaging system could provide a cheap and fast scanning system with a sufficient accuracy for a number of common applications, such as health, robotics, biomechanics, and engineering fields [17,18,19]. By means of its 3D depth sensor, it can detect the distance between the sensor and the object, and it can also provide the 3D model in cloud point format. In the present study, the ability of the Kinect to acquire the shape changes upon the activation of the blade placed behind the PMMA transparent panel was exploited.

In order to control the thermofluid dynamic parameters of the air flow which hit the blade surface, it was essential that the PMMA panels were not to be removed during the test. For this reason, a conventional 3D scanner such as a laser scanner or contact touch probe could not be used. At the same time, these devices are usually unsuitable for real-time applications.

The Kinect was thus placed on a tripod with the IR emitter axis perpendicular to the suction side surface of the blade (aligned with the other cameras), at a distance of approximately 600 mm. Point cloud data were obtained by the freely available software development kit (SDK) provided by Windows, and by using specific open source software (i.e., BLENDER, MESHLAB). Point cloud data were then processed and converted into a polygonal representation of the scanned blade.

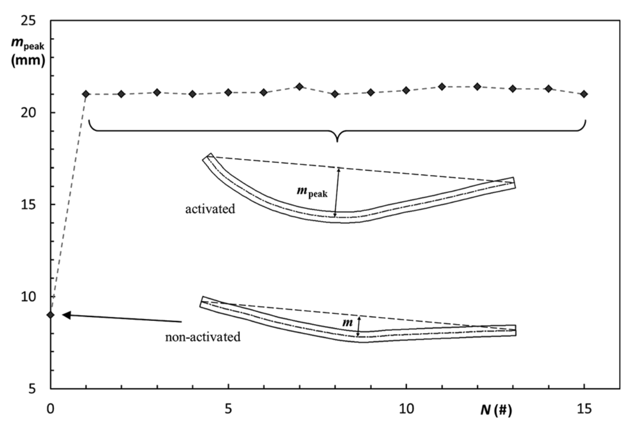

Fig. 2 Blade structure stabilization: airfoil camber variation

Blade Structure Stabilization

In this section, the capability of the SMA strips to recover the memorized bent shape is presented. In order to do this, consecutive thermal cycles were imposed on the same blade structure (polymeric matrix with SMA strips). The first thermal cycle corresponded to the first thermal cycle of the polymeric matrix and the SMA strips. The stabilization tests were conducted by using the SBTF in order to produce the most similar air conditions that characterized the actual application.

Figure 2 reports the trend of the airfoil camber variation during the activation tests. The blade airfoil was evaluated by a CAD reconstruction, provided by using the digital images acquired dur- AQ4 ing the activation test in correspondence to the blade tip view. Experimental results reported in Fig. 2 highlight that the blade stabilization is obtained from the second activation test, in which the maximum camber (reached at the maximum air temperature) is equal to about 21 mm compared to a camber value of 9 mm that characterizes the blade tip airfoil in a nonactivated condition.

The variation in the maximum camber value is less than 1 mm. This small variation encountered during the stabilization tests is clearly reported in Fig. 3, in which the airfoil mean lines at the blade tip are reported. The CAD representation depicted in Fig. 3 shows the blade shape variation and highlights the difference

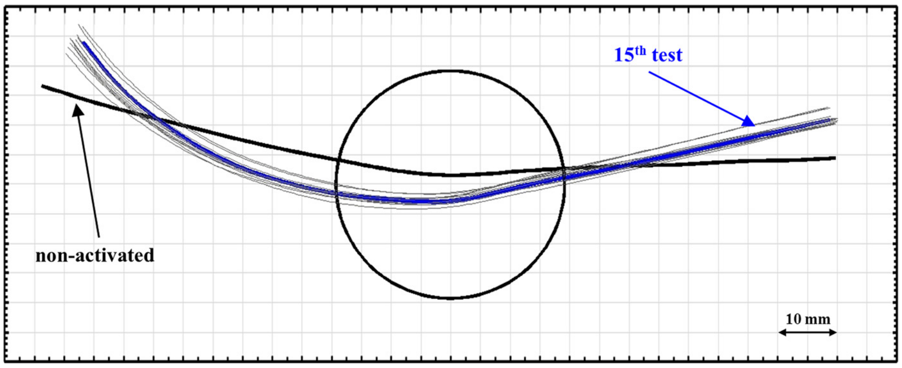

Fig. 3 Evolution of airfoil mean lines at the blade tip

between the nonactivated blade (bold black) and the last stabilization test (bold blue). AQ5

Blade Shape Analysis and Reconstruction

In addition to the camera views discussed in the previous section, the three-dimensional blade shape was acquired during the tests. AQ6 The instantaneous shape acquisition provided by the Kinect sensor allowed the digitalization of the blade shape at the peak temperature instant.

Considering the 3D surfaces, shape measurement techniques are concerned with detecting the geometry information from the image of the measured object. These approaches are known in literature as reverse engineering (RE). In the present application the blade is positioned in the measurement section and a noncontact method (optical) must be used. As reported in Ref. [20], optical methods can often acquire more data in less time, with the advantages of measuring parts without contact. However, the scanning result may not achieve a high accuracy and may have a higher uncertainty when compared to tactile systems [21]. In order to address these issues, the combination of optical measurements and tactile systems, even at different times and locations, can yield a highly accurate 3D representation of the physical object [22,23]. In the present study, tactile systems cannot be used and for this reason, the blade shape detection was carried out by means of (i) a digital image analysis (that provides quantitative and accurate blade detection) and (ii) optical scanning (that provides qualitative blade detection).

Kinect Validation. In order to validate the capability of the Kinect sensor to acquire the three-dimensional blade shape, a preliminary comparison between the acquired Kinect surface and the blade reference CAD geometry was conducted. In Fig. 4, the acquired surface (processed by open source software in order to obtain the polygonal representation) of the nonactivated blade and the blade CAD geometry are superimposed. As shown, the Kinect sensor provided an accurate three-dimensional blade shape. The two entities only differed at the boundary blade regions (especially at the blade tip). However, the deviation was lower than 1 mm. At the edges, the Kinect sensor also detected the blade thickness (as can be seen in Fig. 4), but this detection is less accurate and it was not taken into account during the blade reconstruction. As also reported in Ref. [24], compared to the 2D analysis, the 3D blade detection is less accurate (point clouds data generated by the Kinect sensor were affected by blade surface finishing and the reflection and diffraction of the PMMA panels) than the 2D image captured by a digital camera, but is highly suitable for detecting the instantaneous overall 3D blade shape without disturbing the airflow.

Blade Shape Analysis. As stated above, the Kinect sensor was useful to instantly detect the three-dimensional blade shape. This capability allowed the detection of the blade shapes during the activation test at (i) the start of the thermal cycle, named nonactivated blade (20 °C), (ii) the middle of the thermal cycle, named activated at 60 °C, and (iii) the end of the heating ramp in correspondence to the peak temperature, named activated at 90 °C. The detection referred to a stabilized blade shape after the blade structure stabilization process (see Figs. 2 and 3).

The obtained scanned blades are reported in Fig. 5, in the Kinect surfaces column. As can be seen, the maximum blade deflection is located at the SMA strips housing zone (from 50% to 87% of the blade span, see Fig. 1). In this region, the airfoils experienced a camber variation according to the memorized shape of the SMA strips. In particular, the trailing edge areas appeared more affected by the action of the strips since they were linked with the polymeric structure in the midchord zone. The same assessment can be made by the digital view reported in Fig. 5, in the pressure side view column.

Thanks to the three-dimensional surface provided by the Kinect sensor during the activation tests, it was possible to analyze the different deformations that occurred in the blade shape along its span in a quantitative way. Figure 6 reports the intersection between the suction side surface (Kinect surface) and the four different planes at increasing span: 20%, 50%, 70%, and 90% for a blade height of 34.8 mm, 87.0 mm, 128.8 mm, and 156.6 mm, respectively. The intersection is represented by circular, square and triangular single points for the nonactivated, activated at 60 °C and activated at 90 °C blade shape, respectively, while the trend line improves the readability of the graph.

Since the SMA strips housing zone is located above the midspan, the intersection at 20% of the span showed no differences among the three suction side surfaces. In contrast, the other

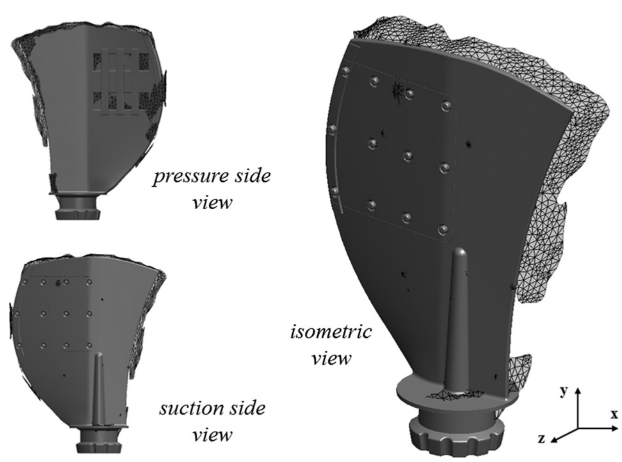

Fig. 4 Blades comparison: Kinect surface versus CAD geometry

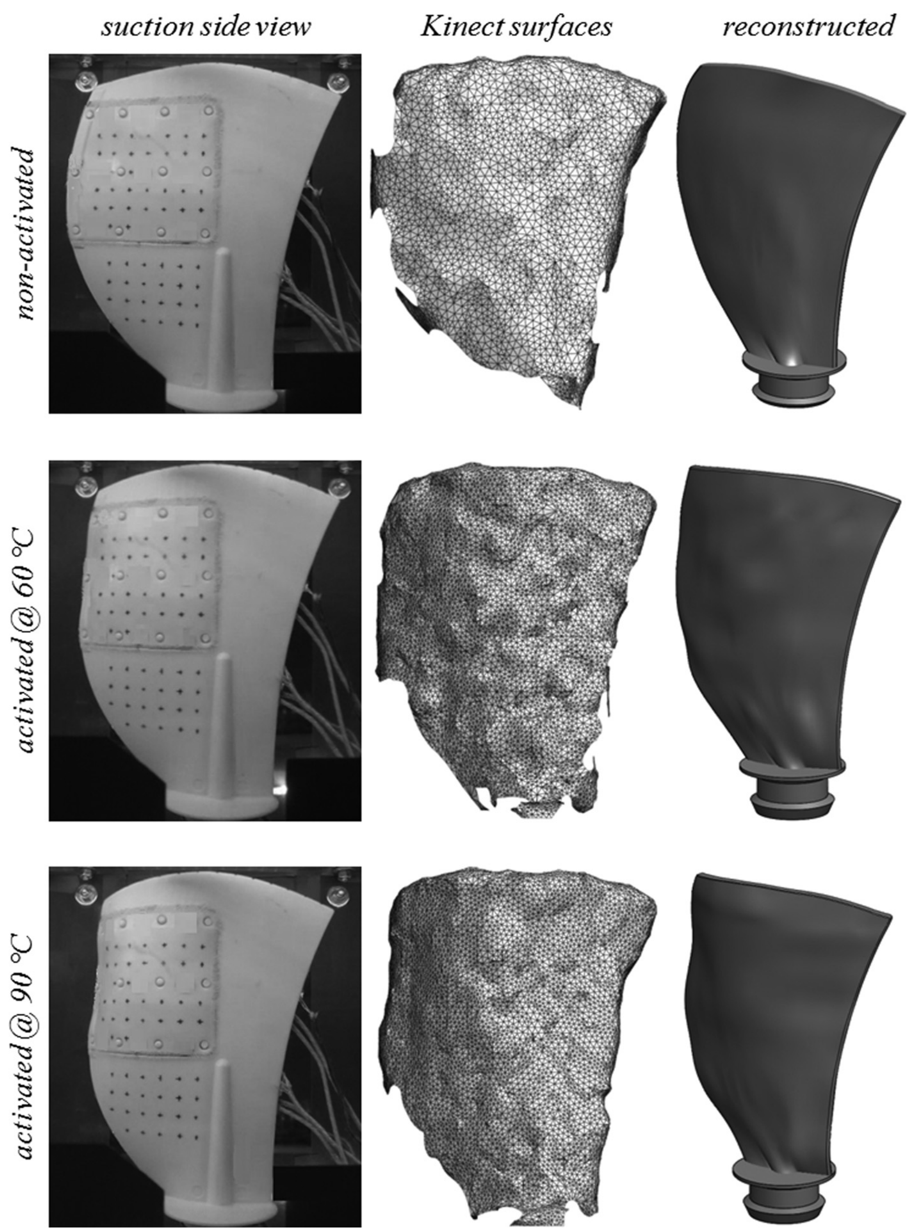

Fig. 5 Digital captions (suction side view), Kinect surfaces and reconstructed blades

intersections showed remarkable deviations among the surfaces. In the leading edge area, the activated blades showed the same deviations with respect to the nonactivated blade. This deviation is about 13 mm, 15 mm, and 20 mm for 50%, 70%, and 90%, respectively. Conversely, in the trailing edge area the activated blades deviation assumes different values. This phenomenon is strongly related to the SMA strips action that imposes a progressive deformation according to the increasing temperature. The deviation between the activated blades is more evident for the 70% and 90% intersections in which the deviation is 10 mm and 15 mm, respectively. As depicted in Fig. 6, blade shape changes (mean line deflection and trailing edge deformation) develop on each blade-to-blade plane as a function of the blade span location. For this reason, the centrifugal force that works in the actual blade's operation does not influence the blade shape modification. SMA strips, embedded in the polymeric matrix, determine the airfoil deflection along the chordwise direction without being affected by the centrifugal force that works along the blade height.

It should be observed that the progressive and continuous blade deformation, due to temperature-driven shape recovery, is directly related to the design of (i) the thermomechanical shape setting SMA strips, (ii) the position of the SMA strips housing zone, and (iii) the polymeric matrix stiffness.

Thanks to these accurate Kinect surfaces the corresponding three-dimensional blade shapes can be achieved. In the third column (reconstructed column) of Fig. 5, the reconstructed blades obtained through a reverse procedure starting from the Kinect surfaces are reported. The parametric CAD representations were generated through B-Splines surface provided by SOLIDWORKS CAD software. By using the reconstructed blade shapes the effects on the fan performance of the aforementioned smooth evolution of the blade shape were studied by means of the CFD analysis presented in the following section. AQ7

CFD Analysis

Starting from the scanned blades, three numerical domains were generated in order to analyze the performance of the fan by means of CFD numerical simulations in nonactivated, activated at 60 °C and activated at 90 °C blade conditions, respectively.

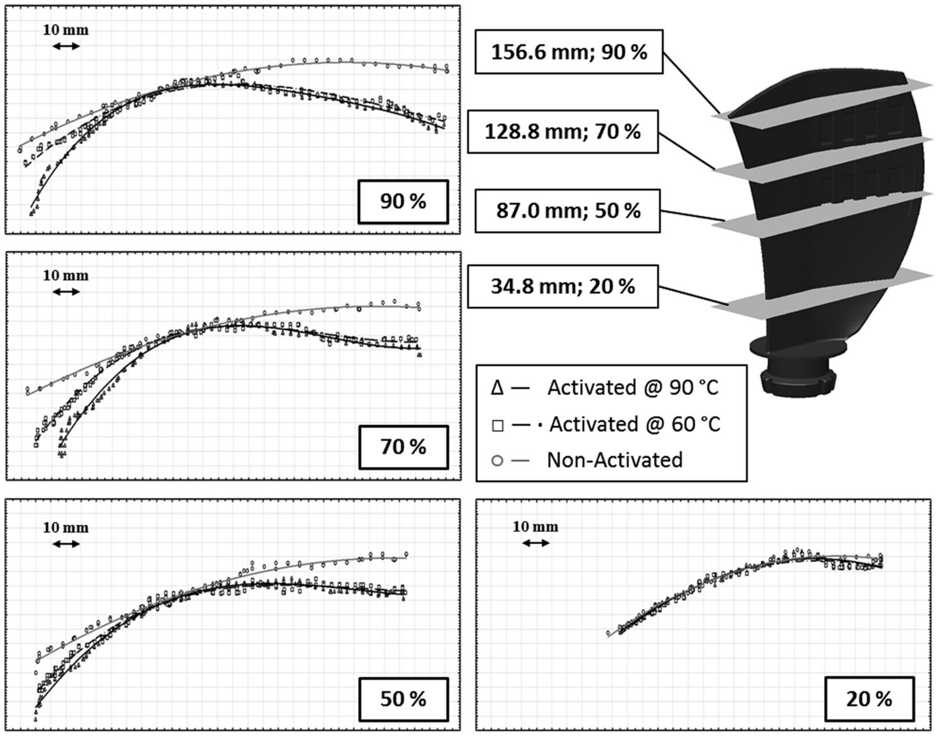

Fig. 6 Suction side deviations at 20%, 50%, 70%, and 90% of the blade span

The numerical simulations were carried out by means of the commercial CFD code ANSYS CFX 15.0. The standard k-ε turbulence model with a scalable wall function was used. This turbulence model well reproduces the performance at the design point in the case of axial turbomachine as reported in Ref. [25]. All the simulations were performed in steady multiple frames of reference AQ8 by using a frozen rotor interface [26,27]. Each numerical domain was composed by three domains: two stationary domains (inlet and outlet duct) and one rotating domain (rotor). A simplified sketch of the numerical domain, with its dimensions, is reported in Fig. 7(*a*). The fan was composed of five blades but only a single passage vane was modeled. The hub to tip ratio was equal to 0.319, while the tip clearance was 5 mm (3.02% of the blade span).

A multiblock hexahedral grid was generated for the numerical domains: (i) 6,024,626 elements for the nonactivated blade, (ii) 6,584,313 elements for the activated at 60 °C blade, and (iii) 6,622,134 for the activated at 90 °C blade. In the three numerical domains, the element size and the mesh refinement close to the wall were comparable and they are showed in Fig. 7(*b*). The y^+ value on the blade surface varies in the range of 4–90 for both of the numerical domains at the best efficiency point.

Boundary Conditions. The numerical simulation was carried out for three different rotational velocities 1000 rpm, 2000 rpm, and 3000 rpm. At the inlet section, the total pressure was imposed equal to 101,325 Pa. At the outlet section, two different conditions were imposed: a relative static pressure for the higher mass flow rate operating condition and an outlet mass flow rate for the lower mass flow rate operating point. Finally, since only a section of the full geometry was modeled, rotational periodic boundary conditions were applied to the lateral surfaces of the flow domain.

Fan Performance. In order to highlight the capability of the blade activation in the modification of the fan performance, the first analysis refers to the comparison between the fan performance with nonactivated blade and the fan performance with the activated at 90 °C blade. The analysis refers to rotational velocities of 3000 rpm and 1000 rpm which correspond to the two extremes of the nominal working rotational velocity range of the fan.

The performance trends in terms of flow coefficient ϕ and pressure coefficient Ψ are reported in Figs. 8 and 9. Differences in terms of pressure and flow coefficient between the maximum and

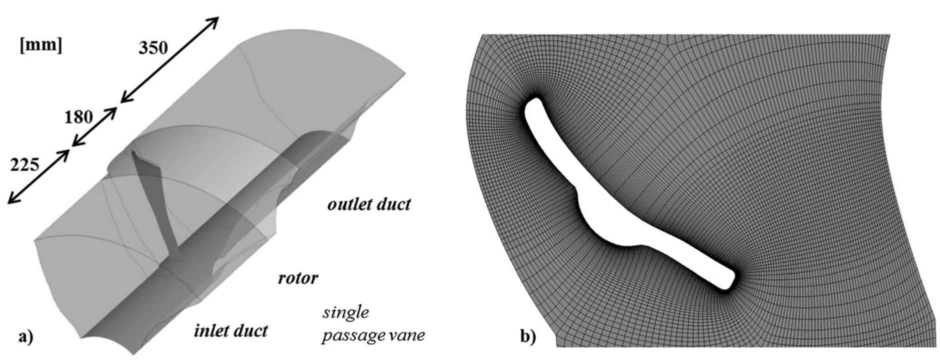

Fig. 7 Numerical domain: (*a*) dimension and domain subdivisions and (*b*) computational mesh around the blade

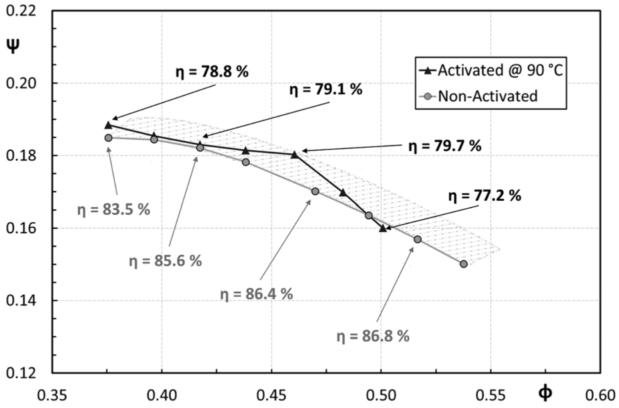

Fig. 8 Fan performance, $n = 3000$ rpm

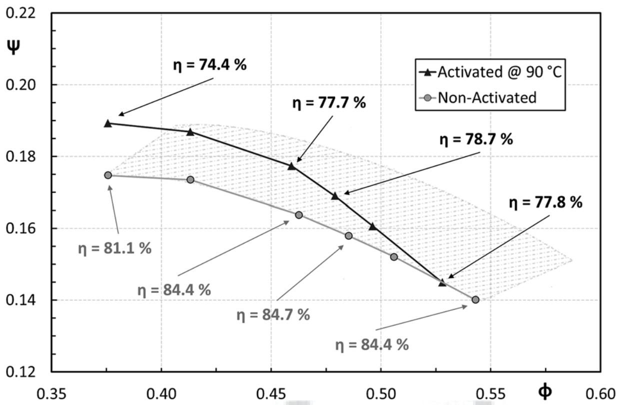

Fig. 9 Fan performance, $n = 1000$ rpm

minimum rotational velocities are due to the different fluid dynamic phenomena that characterized the fan operating conditions in these two ends of the rotational velocity range.

In Fig. 8, the comparison for a rotational velocity equal to 3000 rpm is depicted. The gray region refers to an increase in fan performance of 3%. The fan with the activated at 90 °C blades shows a higher pressure coefficient at the same flow coefficient. In particular, this performance gain is equal to 3% at the best efficiency point of the fan with the activated blades. Figure 8 also reports the values of the efficiency as a function of flow coefficient. The fan efficiency refers to the ratio between fluid power ($Q \cdot \Delta p_0$) and shaft power ($C\ \omega$). The efficiency in the case of the activated at 90 °C blades is less than the case with the nonactivated blades. In Fig. 9, the comparison for a rotational velocity equal to 1000 rpm is depicted. The gray region refers to an increase in the fan performance of 8%. Again, the fan with the activated at 90 °C blades shows a higher pressure coefficient at the same flow coefficient. In this case, the best efficiency point does not correspond to the maximum gain but, for the entire performance trend, the activated at 90 °C blades improve the fan pressure coefficient. Also in this case, the fan efficiency with the activated at 90 °C blades is less than the fan with the nonactivated blade. The camber modification measured in this analysis seems to reduce the fan's stall margin especially for the highest nominal working rotational velocity.

From the following fluid dynamic analysis, it is possible to understand the decrease in the fan efficiency. The analysis is related to the numerical simulation with a rotational velocity equal to 3000 rpm and the comparison refers to the nonactivated and activated at 90 °C blade shapes.

The increase of the pressure coefficient is directly related to the increase of the airfoil camber and leads to a higher flow rate during the fan operation. In fact, when the fluid temperature increases, the blade shape modification generates an increase in the pressure coefficient, and as a result, a higher flow rate through the heat exchanger.

The influence of the blade shape variation is clearly evident from Fig. 10, in which the blade loading and the blade-to-blade velocity contour plots at three spans (25%, 50%, and 75%) are reported. As can be seen from Fig. 10, close to the hub (25% of the blade span), the blade loading and the velocity contour plots are quite similar between the two blades as well as the blade shape. For the other two span positions, the blade shape variation provided by the SMA strips determines the modification of the velocity field, and as a consequence, the modification of the blade loading. The increased airfoil camber provided by the activation of SMA strips determines a lower pressure in the suction side at 50% of the blade span. At the top of the blade (75% of the blade span), the increase in the airfoil camber leads to a pressure decrease in the suction side and to a pressure increase in the pressure side. At 75% of the blade span, there is also an incipient separation, close to the trailing edge of the airfoil, clearly visible in Fig. 10. The increase in the airfoil camber (especially at the top of the blade) determines an increase in the pressure coefficient (as reported in Figs. 8 and 9) but, at the same time, a decrease of the fan efficiency due to the separation on the suction side. The separation is responsible to the reduction of the stall margin as outlined above.

Fan Operating Surfaces. In the last part of this work, the completed fan performance trends are reported. Unlike the results reported in the previous section that referred to the pressure and flow coefficients, in this section the fan performance is presented AQ9

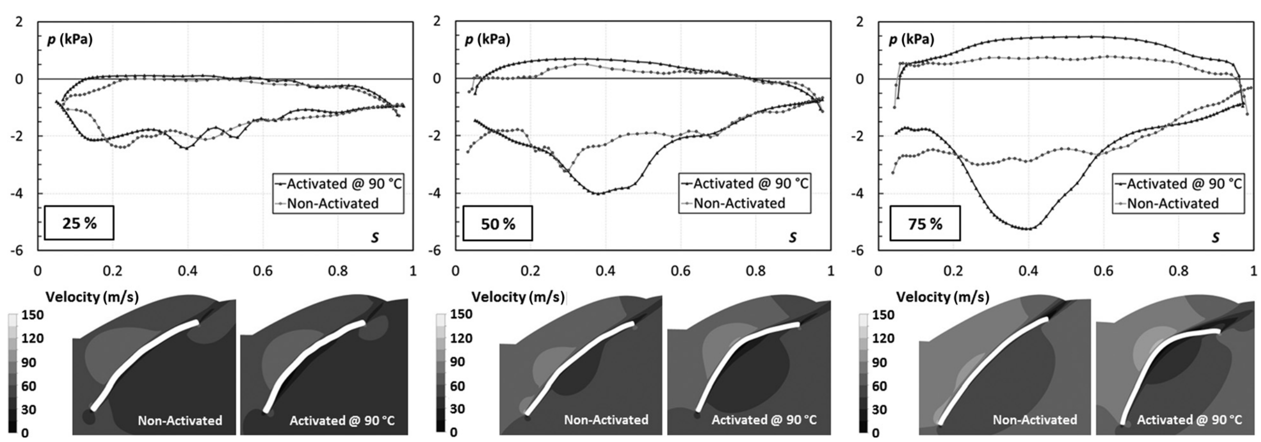

Fig. 10 Blade loading and blade-to-blade velocity field for 25%, 50%, and 75% of the blade span

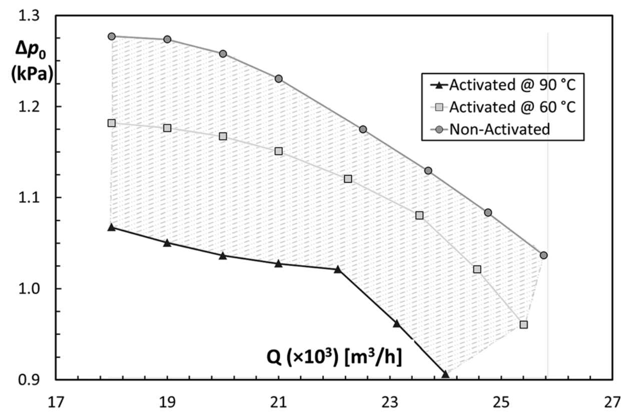

Fig. 11 Fan performance, $n = 3000$ rpm for nonactivated, activated at 60 °C, and activated at 90 °C blades

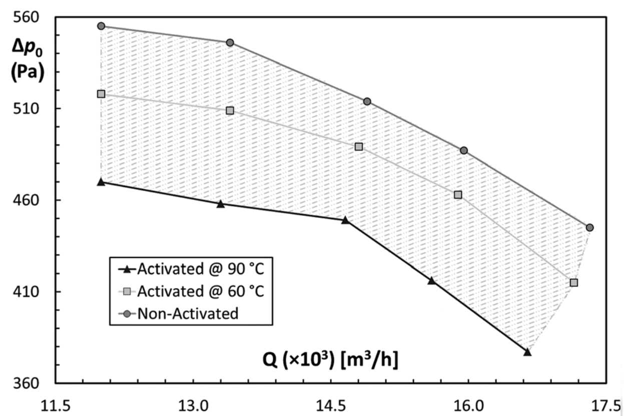

Fig. 12 Fan performance, $n = 2000$ rpm for nonactivated, activated at 60 °C, and activated at 90 °C blades

as a function of the fan rotational velocity and the air temperature and refers to the total pressure increment and the mass flow rate.

The performance of the fan with the three studied blades are reported in Figs. 11–13 for fan rotational velocities equal to 3000 rpm, 2000 rpm, and 1000 rpm, respectively. The gray regions reported in the figures represent the set of the possible fan operating points. In fact, during the actual fan cooling operation, the air temperature changes according to the engine load and/or the effect

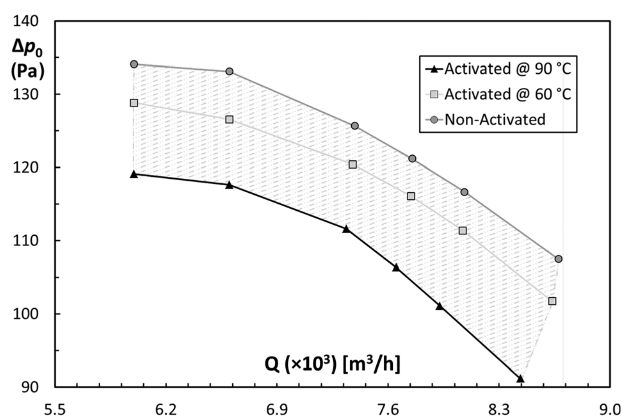

Fig. 13 Fan performance, $n = 1000$ rpm for nonactivated, activated at 60 °C, and activated at 90 °C blades

of the ram air and, at the same time, the fan rotational velocity could be changed due to the engine operation load requirement.

Therefore, the fan equipped with this type of blade follows the thermal/load request of the engine and changes its operating point continuously. The upper performance trends reported in each figure (Figs. 11–13) represent the fan performance with the nonactivated blades for an air temperature equal to 20 °C, while the lower performance trends refer to the fan performance with the activated at 90 °C blades for an air temperature of 90 °C. The fan performance is related to the air temperature and, for this reason, conversely to the performance trend reported in Figs. 8 and 9, the activated fans show a lower performance with respect to the nonactivated fan.

This first numerical analysis confirms the ability of this technology to generate performance variation during operation without sensors and control systems. Fan control by using SMA elements represents an evolution in thermal engine management. The shift from the control of the fan rotational velocity and/or the thermostat to the control of the fan blade shape reflects the modern trend of leaving mathematic control (true/false logic) in favor of more refined control logic. The benefits of using SMA capability to perform actuating functions compared to pneumatic or hydraulic actuators are reduced complexity and improved reliability of the overall mechanical system [17,18]. For this reason, the constant strive for the study and the improvement of the related properties (new alloy compositions, thermomechanical treatments, actuator design, etc.) is of great importance.

The SMA control capability investigated in this work could represent an important upgrade in the field of engine thermal management. In fact, engine emissions, engine fuel consumption, and engine operating life are strictly related to the management of engine coolant temperature. Compared to the typical coolant temperature control systems [1–5], the cooling fan performance controlled by the SMA blades can improve many aspects: (i) the fan performance is directly related to the engine coolant temperature, (ii) the SMA blade control reduces the warm-up time because the mass flow rate provided by the cooling fan continuously changes during the engine heating ramp, (iii) the SMA blade control prevents the engine thermal soak, thanks to the capability of the fan to follow the engine thermal requests, and finally (iv) the downsize of the cooling system and its control devices (for example, the independent electric water pump, valves, and/or the electric actuation of the cooling fan could be suppressed).

Conclusions

In this paper, experimental and numerical analyses on a morphing blade driven by the SMA strips have been reported. Three different blade shapes were used to calculate, by numerical CFD simulations, the upgrade in the axial fan performance generated by the SMA strips activation.

Starting from the preliminary results reported in the first part of this work (related to the control capability of the SMA strips embedded in a polymeric matrix), in this second part the effect of the blade shape modification on a fan performance has been studied.

The experimental tests on a single blade were performed by using a purpose-built wind tunnel and the blade shape modifications were acquired by using obtained thanks to Kinect sensor. The thermal gradients (for the heating and cooling ramp), realized by means of an electric heater, were in line with those which take place in automotive cooling circuits. Thanks to the challenging and innovative three-dimensional blade surface capture system provided by Kinect sensor it was possible to digitalize the blade shape changes during the activation tests. This noncontact sensor can measure the instantaneous three-dimensional shape through the PMMA panels without affecting the thermal and flow wind tunnel conditions.

After an investigation of the blade structure stabilization, the stabilized blade shapes were scanned and used to provide the CFD analyses in order to highlight the differences in the fan performance due to the different shapes of the blade.

The analyses showed that the activated blades led to an increase in the fan pressure ratio up to 8%, compared to the nonactivated blade. A blade loading analysis compared to the velocity analysis revealed that the increment in the fan performance was directly related to the blade shape modification that occurs in the SMA strip housing zone.

This preliminary study shows that the opportunity to generate an innovative passive control system applied to an axial fan is realizable. The innovative activation method proposed is suitable to modify the performance in agreement with the requests of the circuit.

Future developments will concern (i) the optimization of the behavior of the SMA elements by means of specific shape-setting treatments, (ii) the study of the shape recovery behavior in subsequent activation thermal cycles to improve the blade structure stabilization, (iii) the assessment of the reliability of the noncontact detection method for the analysis of the blade shape modification, and (iv) the blade aerodynamic design in order to increase fan performance and stall margin. The developments of a blade design will be dedicated to the enhancement of fan efficiency in order to reduce the diverted engine power at full load.

Acknowledgment

The authors wish to thank Fratelli Rosati s.r.l. of Leinì (Torino-Italy) for the financial and technical support in this research.

The authors would like to dedicate this work in memory of Engineer Guido Rosati, whose guidance and encouragement have been of great importance to achieve the present results.

Nomenclature

C = torque
m = camber
n = rotational velocity
N = cycle
p = pressure
Q = volume flow rate
S = blade loading coordinate
t = time
T = temperature
U_t = blade velocity at the tip
V_a = axial flow velocity
y^+ = nondimensional wall distance

Greek Symbols

Δ = increment
η = efficiency
$\phi = = V_a/U_t$ flow coefficient
$\Psi = = \Delta p_0/\rho U_t^2$ pressure coefficient
ω = angular velocity

Subscripts and Superscripts

peak = peak (referred to the camber)
0 = total (referred to the pressure)

Acronyms

CFD = computational fluid dynamics
IR = infrared
PMMA = polymethyl methacrylate
PVC = polyvinyl chloride
RE = reverse engineering
SBTF = single blade test facility
SDK = software development kit
SMA = shape memory alloy

References

[1] Lin, W., and Sunden, B., 2010, "Vehicle Cooling Systems for Reducing Fuel, Consumption and Carbon Dioxide: Literature Survey," SAE Technical Paper No. 2010-01-1509.
[2] Chalgren, R. D., 2004, "Thermal Comfort and Engine Warm-Up Optimization of a Low-Flow Advanced Thermal Management System," SAE Technical Paper No. 2004-01-0047.
[3] Nessim, W., Zhang, F., Changlu, Z., and Zhenxia, Z., 2012, "A Simulation Study of an Advanced Thermal Management System for Heavy Duty Diesel Engines," 2012 International Conference on Mechanical Engineering and Material Science (MEMS 2012), pp. 287–290.
[4] Lehner, C., Parker, G., Arici, O., and Johnson, J., 2006, "Design and Development of a Model Based Feedback Controlled Cooling System for Heavy Duty Diesel Truck Applications Using a Vehicle Engine Cooling System Simulation," SAE Technical Paper No. 2001-01-0336.
[5] Baniasadi, E., Aydin, M., Dincer, I., and Naterer, G. F., 2013, "Computational Aerodynamic Study of Automotive Cooling Fan in Blocked Conditions," Eng. Appl. Comput. Fluid Mech., **7**(1), pp. 66–73. AQ10
[6] Fortini, A., Suman, A., Aldi, N., Merlin, M., and Pinelli, M., 2016, "A Shape Memory Alloy-Based Morphing Axial Fan Blade—Part I: Blade Structure Design and Functional Characterization," ASME J. Eng. Gas Turbines Power, **138**(2), p. 022601.
[7] Kim, K. B., Choi, K. W., Lee, K. H., and Lee, K. S., 2010, "Active Coolant Control Strategies in Automotive Engines," Int. J. Automot. Technol., **11**(6), pp. 767–772.
[8] Pang, S. C., Kalam, M. A., Masjuki, H. H., and Hazrat, M. A., 2012, "A Review on Air Flow and Coolant Flow Circuit in Vehicles Cooling System," Int. J. Heat Mass Transfer, **55**(■), pp. 6295–6306.
[9] Oliet, C., Oliva, A., Castro, J., and Pérez-Segarra, C. D., 2007, "Parametric Studies on Automotive Radiators," Appl. Therm. Eng., **27**(■), pp. 2033–2043.
[10] Hallqvist, T., 2008, "The Cooling Airflow of Heavy Trucks–A Parametric Study," SAE Technical Paper No. 2008-01-1171.
[11] Mao, S., Feng, Z., and Michaelides, E. E., 2010, "Off-Highway Heavy-Duty Truck Under-Hood Thermal Analysis," Appl. Therm. Eng., **30**(13), pp. 1726–1733.
[12] Pang, S. C., Kalam, M. A., Masjuki, H. H., Badruddin, I. A., Ramli, R., and Hazrat, M. A., 2012, "Underhood Geometry Modification and Transient Coolant Temperature Modelling for Robust Cooling Networks," Int. J. Mech. Mater. Eng., **7**(■), pp. 251–258.
[13] Senatore, A., Cardone, M., Buono, D., and Dominici, A., 2008, "High Performance Engine Warm-Up Thermo-Fluid-Dynamic Analysis," IMECE2008, Boston, MA, Oct. 31–Nov. 6, pp. 305–313.
[14] Sofla, A. Y. N., Meguid, S. A., Tan, K. T., and Yeo, W. K., 2010, "Shape Morphing of Aircraft Wing: Status and Challenges," Mater. Des., **31**(3), pp. 1284–1292.
[15] Epps, J., and Chopra, I., 2001, "In-Flight Tracking of Helicopter Rotor Blades Using Shape Memory Alloy Actuators," Smart Mater. Struct., **10**(1), pp. 104–111.
[16] Lachenal, X., Daynes, S., and Weaver, P. M., 2013, "Review of Morphing Concepts and Materials for Wind Turbine Blade Applications," Wind Energy, **16**(2), pp. 283–307.
[17] Gonzalez-Jorge, H., Riveiro, B., Vazquez-Fernandez, E., Martínez-Sánchez, J., and Arias, P., 2013, "Metrological Evaluation of Microsoft Kinect and Asus Xtion Sensors," Measurement, **46**(6), pp. 1800–1806.
[18] Khoshelham, K., and Elberink, S. O., 2012, "Accuracy and Resolution of Kinect Depth Data for Indoor Mapping Applications," Sensors, **12**(12), pp. 1437–1454.
[19] Yue, H., Chen, W., Wu, X., and Liu, J., 2014, "Fast 3D Modeling in Complex Environments Using a Single Kinect Sensor," Opt. Lasers Eng., **53**(■), pp. 104–111. AQ11
[20] Schwenke, H., Neuschaefer-Rube, U., Pfeifer, T., and Kunzmann, H., 2002, "Optical Methods for Dimensional Metrology in Production Engineering," CIRP Annu.-Manuf. Technol., **51**(2), pp. 685–699.
[21] Sansoni, G., and Docchio, F., 2005, "In-Field Performance of an Optical Digitizer for the Reverse Engineering of Free-Form Surfaces," Int. J. Adv. Manuf. Technol., **26**(■), pp. 1353–1361.
[22] Carbone, V., Carocci, M., Savio, E., Sansoni, G., and De Chiffre, L., 2001, "Combination of a Vision System and a Coordinate Measuring Machine for the Reverse Engineering of Free-Form Surfaces," Int. J. Adv. Manuf. Technol., **17**(4), pp. 263–271.
[23] Chen, L.-C., and Lin, G. C. I., 1997, "An Integrated Reverse Engineering Approach to Reconstructing Free-Form Surfaces," Comput. Integr. Manuf. Syst., **10**(1), pp. 49–60.
[24] Fortini, A., Suman, A., Merlin, M., and Garagnani, G. L., 2015, "Morphing Blades With Embedded SMA Strips: An Experimental Investigation," Mater. Des., **85**(■), pp. 785–795.
[25] Cornelius, C., Biesinger, T., Galpin, P., and Braune, A., 2014, "Experimental and Computational Analysis of a Multistage Axial Compressor Including Stall Prediction by Steady and Transient CFD Methods," ASME J. Turbomach., **136**(■), p. 061013.
[26] Abdullah, E. J., Bil, C., and Watkins, S., 2009, "Application of Smart Materials for Adaptive Airfoil Control," AIAA Paper No. 2009-1359.
[27] Mertmann, M., and Vergani, G., 2008, "Design and Application of Shape Memory Actuators," Eur. Phys. J. Spec. Top., **158**(1), pp. 221–230.